CO Methanation

International Edition: DOI: 10.1002/anie.201903882
German Edition: DOI: 10.1002/ange.201903882

Morphology-Engineered Highly Active and Stable Ru/TiO_2 Catalysts for Selective CO Methanation

Shilong Chen[+], Ali M. Abdel-Mageed[+], Dan Li, Joachim Bansmann, Sebastian Cisneros, Johannes Biskupek, Weixin Huang, and R. Jürgen Behm**

Abstract: *Ru/TiO_2 catalysts exhibit an exceptionally high activity in the selective methanation of CO in CO_2- and H_2-rich reformates, but suffer from continuous deactivation during reaction. This limitation can be overcome through the fabrication of highly active and non-deactivating Ru/TiO_2 catalysts by engineering the morphology of the TiO_2 support. Using anatase TiO_2 nanocrystals with mainly {001}, {100}, or {101} facets exposed, we show that after an initial activation period Ru/TiO_2-{100} and Ru/TiO_2-{101} are very stable, while Ru/TiO_2-{001} deactivates continuously. Employing different operando/in situ spectroscopies and ex situ characterizations, we show that differences in the catalytic stability are related to differences in the metal–support interactions (MSIs). The stronger MSIs on the defect-rich TiO_2-{100} and TiO_2-{101} supports stabilize flat Ru nanoparticles, while on TiO_2-{001} hemispherical particles develop. The former MSIs also lead to electronic modifications of Ru surface atoms, reflected by the stronger bonding of adsorbed CO on those catalysts than on Ru/TiO_2-{001}.*

The selective methanation of CO in CO_2- and H_2-rich reformates has attracted growing interest due to its potential in the ultrapurification of H_2 for proton-exchange membrane fuel cells (PEMFCs).[1,2] Oxide-supported Ru catalysts were found as highly active and selective catalysts, especially at low temperatures.[3–6] Recent findings on Ru nanoparticles (NPs) on different oxide supports[7–13] indicated that their intrinsic selectivity for CO methanation is mainly determined by the Ru particle size, while the activity varied with the support reducibility[11] and, for Ru/TiO_2, with the BET specific surface area[9] and the associated variations in metal–support interactions (MSIs). The activity of Ru/TiO_2 catalysts was reported to exceed those of isostructural Ru/Al_2O_3 and Ru/ZrO_2 catalysts by a factor of ≈ 5.[11] Unfortunately, Ru/TiO_2 catalysts showed a continuous deactivation, which was mainly attributed to a slow growth of Ru nanoparticles.[10] Thus, designing a non-deactivating Ru/TiO_2 catalyst is a crucial issue for possible applications.

In addition to varying the surface area of the support, engineering of their morphology has been recognized as an effective approach to modify the MSIs in oxide-supported catalysts, which can affect both the size and shape of the metal NPs and the catalytic performance of these catalysts.[14–17] Distinct TiO_2 morphology effects were reported for Au/TiO_2 catalysts in the propylene epoxidation and CO oxidation reactions.[18,19] Here, we apply this approach for the selective methanation of CO on Ru/TiO_2 catalysts, employing TiO_2 nanocrystals (NCs) predominantly exposing {001}, {100}, and {101} facets. The success of this approach will be demonstrated in the following.

Anatase TiO_2-{001}, TiO_2-{100}, and TiO_2-{101} NCs with uniform morphologies were prepared via a hydrothermal procedure described elsewhere.[20,21] The morphologies of the resulting NCs (Figure 1 a–c) agree well with previous

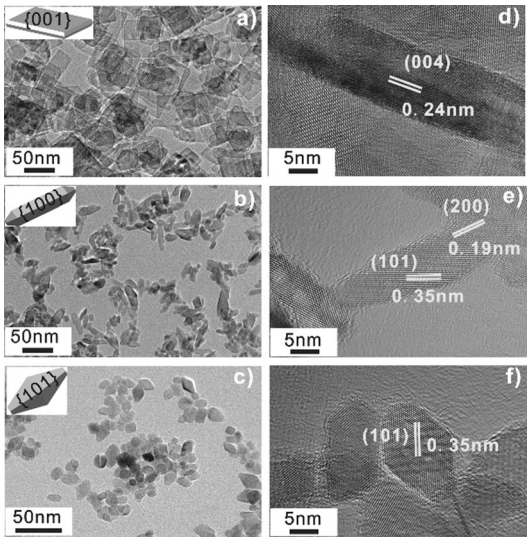

Figure 1. Representative TEM images of as-synthesized anatase TiO_2 nanocrystals: a) TiO_2-{001}, b) TiO_2-{100}, c) TiO_2-{101}, d–f) lattice fringes of TiO_2 NCs in HR-TEM. Additional TEM images of TiO_2 nanocrystals are shown in Figure S3.

[*] Dr. S. Chen,[+] Dr. A. M. Abdel-Mageed,[+] Dr. J. Bansmann, M. Sc. S. Cisneros, Prof. Dr. R. J. Behm
Institute of Surface Chemistry and Catalysis
Ulm University
89069 Ulm (Germany)
E-mail: juergen.behm@uni-ulm.de
D. Li, Prof. Dr. W. Huang
Hefei National Laboratory for Physical Sciences at the Microscale, Key Laboratory of Surface and Interface Chemistry and Energy Catalysis of Anhui Higher Education Institutes and Department of Chemical Physics, University of Science and Technology of China
230026 Hefei (P. R. China)
E-mail: huangwx@ustc.edu.cn
Dr. J. Biskupek
Central Facility for Electron Microscopy
Ulm University
89069 Ulm (Germany)
[+] These authors contributed equally to this work.
Supporting information and the ORCID identification number(s) for the author(s) of this article can be found under: https://doi.org/10.1002/anie.201903882.

results;[18,22,23] the fractions of the dominant facets are around 80–100% (see the Supporting Information (SI)). The BET specific surface areas of the TiO_2 NCs are all around 100 $m^2 g^{-1}$ (Table S1). Using these support materials, Ru/TiO_2 catalysts with Ru loadings around 1.9 wt% (Table S1) were prepared by incipient wetness impregnation. In X-ray diffraction (XRD) we only detected reflections characteristic for anatase TiO_2 (Figure S2).

The catalytic activity of the three Ru/TiO_2 catalysts was first evaluated in a medium CO content reformate gas (SR-ref 6000: 6000 ppm CO, 15.5% CO_2, 3% N_2 and H_2 balance) (Figure 2a). The selectivity for CO methanation in this

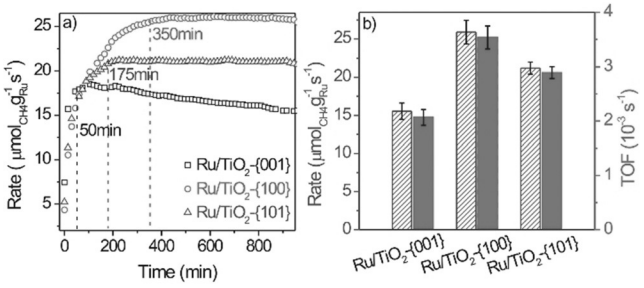

Figure 2. a) Temporal evolution of the Ru mass-normalized reaction rate and b) steady-state rates (hatched) and the corresponding turnover frequencies (TOFs, gray) in SR-ref 6000 reformate at 190°C.

reformate is essentially 100%, which was previously explained by a site-blocking mechanism.[9,10] For the Ru/TiO_2-{001} catalyst, the Ru mass-normalized reaction rate increases from 7.4 to 18.5 $\mu mol_{CH_4}\, g_{Ru}^{-1}\, s^{-1}$ during the first 50 min, but then decreased continuously with time on stream, reaching $\approx$15.5 $\mu mol_{CH_4}\, g_{Ru}^{-1}\, s^{-1}$ (TOF: $2.1 \times 10^{-3}\, s^{-1}$) after 950 min (Figure 2b). The Ru/TiO_2-{100} and Ru/TiO_2-{101} catalysts exhibited much longer activation phases, reaching the highest activity after 350 min (26 $\mu mol_{CH_4}\, g_{Ru}^{-1}\, s^{-1}$) and after 175 min (21 $\mu mol_{CH_4}\, g_{Ru}^{-1}\, s^{-1}$), respectively. Moreover, neither catalyst showed any measurable deactivation (Figure 2b). The high stability of these catalysts is strikingly different from the trend of previously reported standard Ru/TiO_2 catalysts with mixed surface morphologies, which showed about 20% deactivation under identical conditions.[9–11] To the best of our knowledge, these Ru/TiO_2-{100} and Ru/TiO_2-{101} catalysts are the first examples of Ru/TiO_2 catalysts that are highly active and non-deactivating under these conditions. Also, these demonstrate pronounced effects of the TiO_2 morphology on the catalytic performance of Ru/TiO_2 catalysts.

Additional measurements performed with low CO contents (0.01% CO, 15.5% CO_2, 3% N_2 and H_2 balance) furthermore confirmed that also under conditions where CO adsorption does not block the surface, the inherent selectivity is close to 100% (see Figure S4b), in good agreement with previous findings for similar Ru particle sizes.[7,8] Furthermore, to test temperature effects on the CO methanation we performed measurements in SR-ref 6000, varying the temperature from 170 to 300°C. We found that all three catalysts are 100% selective for CO methanation up to 230°C, where the CO_2 methanation sets in (Figure S5).

To elucidate the physical origin of these differences in reaction behavior we tested structural changes of the Ru/TiO_2 catalysts during the reaction and after exposure for 10 and for 1000 min to the reaction gas at 190°C, respectively, by TEM imaging (Figures S6–S10). First of all, the morphologies of the TiO_2 NCs in the Ru/TiO_2 catalysts are well preserved during the reaction. Second, the Ru particle size distributions of all Ru/TiO_2 catalysts did not change significantly during 1000 min on stream. The average sizes of Ru NPs increased slightly from 1.2 to 1.3 nm for Ru/TiO_2-{001}, from 1.2 to 1.35 nm for Ru/TiO_2-{100}, and from 1.25 to 1.4 nm for the Ru/TiO_2-{101} catalyst (Figure S11). Third, we evaluated the shape of the NPs and possible changes therein in the TEM images. We did this by determining the ratio between the short diameter (R1) and the long diameter (R2) of the two-dimensional projection of the individual Ru NPs. Spherical or quasi-spherical particles always show a ratio of 1, while flat particles show lower values on average (Figure 3a).[10,11] After 10 min reaction (Figure 3b–d), the fraction of Ru particles with ratios $\leq$0.8 follows the order Ru/TiO_2-{101} (76.2%) > Ru/TiO_2-{100} (71.9%) > Ru/TiO_2-{001} (63.0%), indicating

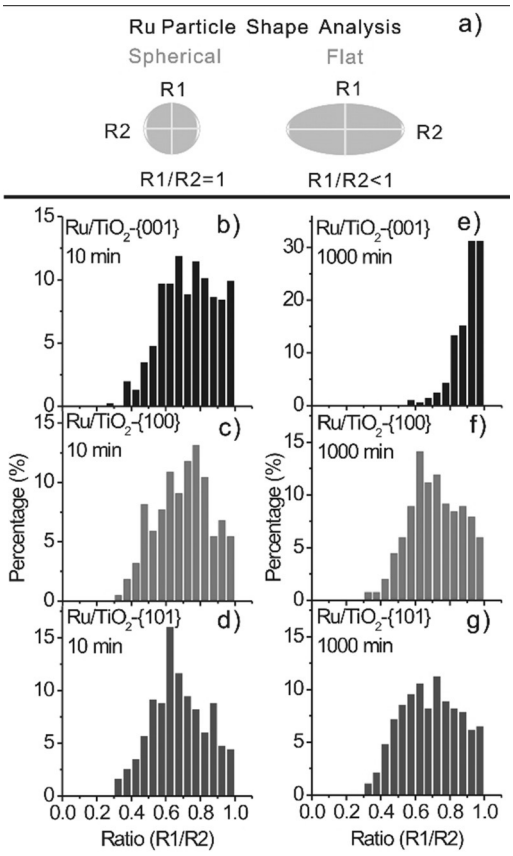

Figure 3. a) Schematic presentation of the particle shape analysis based on the TEM images. The frequencies of the Ru particle diameter ratios R1/R2 of b,e) Ru/TiO_2-{001}, c,f) Ru/TiO_2-{100}, d,g) Ru/TiO_2-{101} catalysts after reaction for 10 min (left panels: (b, c, d)) and for 1000 min (right panels: (e, f, g)) in SR-ref 6000 reformate at 190°C. TEM images used for size and shape evaluation are shown in Figures S5–S9.

that more flat Ru particles are present on Ru/TiO_2-{100} and Ru/TiO_2-{101} than on Ru/TiO_2-{001}. After 1000 min reaction, the fraction of Ru particles with ratios ≤ 0.8 decreased to 9.4% on Ru/TiO_2-{001}, while on Ru/TiO_2-{100} and on Ru/TiO_2-{101} these ratios did not change, but remained stable at 70% (Ru/TiO_2-{100}) and 72% (Ru/TiO_2-{101}) (Figure 3e–g). Thus, on Ru/TiO_2-{100} and Ru/TiO_2-{101} the flat Ru NPs are more resistant to shape changes during reaction than on Ru/TiO_2-{001}, while for all catalysts the Ru NPs grow only slightly in size. These observations indicate much stronger Ru–TiO_2 interactions in Ru/TiO_2-{100} and Ru/TiO_2-{101} than in Ru/TiO_2-{001}.

The coordination environment of the Ru species on the Ru/TiO_2-{001} and Ru/TiO_2-{100} catalysts and changes therein during reaction were followed by time-resolved operando Ru K-edge EXAFS. Representative Fourier transforms of the spectra (black lines) and the resulting fits (gray lines) are shown in Figure 4a,b. Details of the EXAFS evaluation and the corresponding fit parameters as well as the resulting coordination numbers are summarized in the Experimental Section and in Tables S2 and S3 in the SI. After calcination, the Ru/TiO_2-{001} and Ru/TiO_2-{100} catalysts show significant contributions of a Ru–O coordination shell at distances of (2.15 ± 0.03) Å and (2.11 ± 0.03) Å, respectively, with Ru–O coordination numbers ($CN_{Ru\text{-}O}$) of 1.3 ± 0.3 and 2.9 ± 0.6. Upon switching to the reaction gas, the $CN_{Ru\text{-}O}$ of the Ru/TiO_2-{001} catalyst decreased rapidly, being negligible already after 7 min. In turn, the corresponding $CN_{Ru\text{-}Ru}$ values increased quickly to 3.8 ± 0.8 after 7 min and then further grew up to 6.6 ± 1.0 after 450 min. Hence, while reduction of the Ru oxide NPs is rapid, structural changes in the metallic NPs continue over longer times. For Ru/TiO_2-{100}, reduction was also rapid, with the $CN_{Ru\text{-}O}$ value decreasing from 2.9 ± 0.6 after calcination to 1.1 ± 0.3 after 6 min, and 0.1 ± 0.1 after 60 min (see Table S3, for details). In this case, however, the $CN_{Ru\text{-}Ru}$ characteristic for metallic Ru species, increased only from 1.2 ± 0.5 after 6 min to about 3.7 ± 0.8 after 60 min and then remained about constant for over 450 min. These results indicate significant differences in the size/shape of the resulting Ru NPs for the two catalysts.

Assuming hemispherical particle shapes, the $CN_{Ru\text{-}Ru}$ values listed above can be converted into Ru particle sizes.[24] For Ru/TiO_2-{001}, these would grow from (0.45 ± 0.1) nm ($CN_{Ru\text{-}Ru}$: 3.8 ± 0.8) to (0.9 ± 0.1) nm ($CN_{Ru\text{-}Ru}$: 6.6 ± 1.0) during reaction. This differs significantly from the TEM results, which showed only a slight growth of the Ru particle size from 1.2 nm to 1.3 nm. For Ru/TiO_2-{100}, in contrast, both TEM and EXAFS reveal little change in Ru NP size after the initial reduction phase, and the $CN_{Ru\text{-}Ru}$ value remains at 3.7 ± 0.8 at extended reaction times (> 45 min). It is well known that for very small NPs TEM and EXAFS analysis can result in rather different particle sizes, since EXAFS is especially sensitive for very small particles, while in TEM these may be below the resolution limit.[25] This should, however, apply equally for both catalysts. We therefore assume that the pronounced apparent increase in the EXAFS-based particle size observed for Ru/TiO_2-{001} results mainly from a change in particle shape during reaction, from flat to hemispherical, rather than from an increase in particle size. For Ru/TiO_2-{100}, in contrast, the data indicate that there is little growth in particle size after the initial reduction phase and that there is also no change in shape towards a more hemispherical form. In summary, the EXAFS data fully support our previous TEM based conclusion that the deactivation of the Ru/TiO_2-{001} catalyst during reaction is mainly due to a change in the shape of the Ru NPs, from flat to hemispherical, while this does not occur for Ru/TiO_2-{100}.

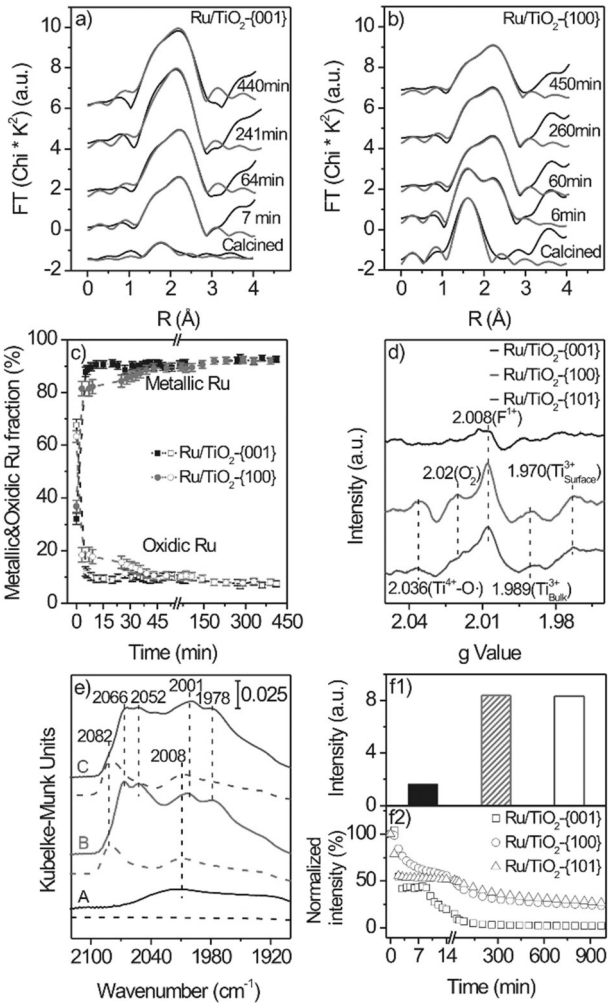

Figure 4. Fourier transformed EXAFS spectra in R-space recorded at the Ru K-edge after calcination in N_2 and at different reaction times on a) Ru/TiO_2-{001} and b) Ru/TiO_2-{100} (black lines: measured EXAFS data, gray lines: fit data). c) Fractions of metallic Ru (filled symbols) and oxidic Ru species (RuO_2 and $RuCl_3$: empty symbols) as a function of time derived from a LCA analysis of XANES spectra of Ru/TiO_2-{001} and Ru/TiO_2-{100}. d) EPR spectra of three Ru/TiO_2 catalysts after reaching steady state during reaction. e) Steady-state DRIFT spectra recorded during reaction (solid lines) and after subsequent isothermal desorption in N_2 (dashed lines) of Ru/TiO_2-{001} (A), Ru/TiO_2-{100} (B), and Ru/TiO_2-{101} (C), respectively. f1) Total intensity of all CO_{ad}-related bands in the DRIFT spectra on Ru/TiO_2-{001} (filled), Ru/TiO_2-{100} (hatched), and Ru/TiO_2-{101} (blank) during reaction under steady-state conditions. f2) Time evolution of the normalized band intensities (100% at the beginning) related to all CO_{ad} species during isothermal desorption in N_2. All reaction and desorption experiments were performed at 190°C.

Information on the chemical state of the Ru NPs was obtained from the near-edge region of the X-ray absorption spectra (Figure S12). The results of a linear combination analysis (LCA) of the XANES region for both catalysts (Figure S13) indicated that in the calcined Ru/TiO_2-{001} and Ru/TiO_2-{100} catalysts the Ru species are composed of $\approx 70\,\%$ oxidic and $\approx 30\,\%$ metallic Ru species (Figure 4c). During reaction, the content of metallic Ru species in Ru/TiO_2-{001} increased from 32.0 % to 90.0 % after 10 min and did not change much at extended reaction times. For Ru/TiO_2-{100} the reduction process was slower:. After 10 min the content of metallic Ru species increased from 37.0 % to 82.0 % and about 50 min was required for it to reach to 90 %. After that, it remained about roughly unchanged. The observation of a longer reduction phase for Ru/TiO_2-{100} fits well with the significantly longer activation phase on this catalyst and reflects a strong impact of surface morphology on the reduction of oxidized Ru species.

XP spectra recorded on the spent catalysts (Figure S14) show that the Ru $3d_{5/2}$ BEs of all catalysts are between 280.0 and 280.2 eV, a typical value for metallic Ru NPs,[9] and that the Ti $2p_{3/2}$ BEs are around (458.8 ± 0.1) eV, which is about 0.4 eV lower than the standard binding energy of Ti^{4+} in fully oxidized TiO_2.[9–11] This points to a partial reduction of the TiO_2 supports, in agreement with previous findings.[11]

The presence of O-vacancies during reaction is demonstrated also by electron paramagnetic resonance (EPR) spectroscopy. EPR spectra recorded on the spent Ru/TiO_2 catalysts (see Figure 4d and the Experimental Section in the SI for details) reveal for all catalysts a distinct feature at $g = 2.008$, which is related to O-vacancies with one electron (F^{1+} color center) located in the subsurface or bulk regions of TiO_2.[22,26] Ru/TiO_2-{100} and Ru/TiO_2-{101} exhibit additional features at $g = 2.03$, which had been assigned to O_2^- species resulting from the adsorption of O_2 on F^{1+} color centers at the TiO_2 surface,[22,27] and also at $g = 1.989$ and $g = 1.970$. The latter signals had previously been assigned to bulk ($Ti^{3+}{}_{bulk}$) and surface ($Ti^{3+}{}_{surface}$) Ti^{3+} species, respectively.[22,27] In contrast, on Ru/TiO_2-{001}, we did not detect any additional surface defect signals. Hence, Ru/TiO_2-{100} and Ru/TiO_2-{101} show a significantly higher concentration of surface and bulk defects than Ru/TiO_2-{001}, which can enhance the Ru–TiO_2 interactions and thus stabilize flat Ru NPs.

Information on the adsorption properties of the Ru NPs and their variation with TiO_2 morphology was obtained by time-resolved in situ diffuse reflectance FTIR spectroscopy (DRIFTS), following the adsorption of CO during reaction. Spectra of three Ru/TiO_2 catalysts at steady state during reaction are shown in Figure 4e as solid lines; complete time sequences of the resulting DRIFT spectra and the time evolution of the CO_{ad} coverage are presented in Figure S15. All Ru/TiO_2 catalysts exhibit characteristic vibrational bands of CO_{ad} species in the range from 1920 to 2150 cm^{-1}, which change with time and differ with the morphology of TiO_2. The bands at 1960–2060 cm^{-1} are commonly assigned to on-top adsorbed CO on Ru NPs,[28,29] with the higher frequency band around 2060 cm^{-1} corresponding to CO_{ad} on low-coordination Ru sites and the lower frequency bands of 1960–2050 cm^{-1} corresponding to CO_{ad} on high-coordination Ru surface atoms, respectively.[29] The bands at around 2080 and 2140 cm^{-1} were attributed previously to Ru–multicarbonyl species.[28,29] Ru/TiO_2-{100} and Ru/TiO_2-{101} show similar CO adsorption characteristics with CO_{ad} occupying low- and high-coordination Ru surface sites, while Ru/TiO_2-{001} only shows CO_{ad} on high-coordination Ru surface atoms, as would be expected for hemispherical/round Ru NPs. Furthermore, Ru/TiO_2-{100} and Ru/TiO_2-{101} show similar CO_{ad} absorption intensities and thus similar CO_{ad} coverages, while on Ru/TiO_2-{001} it is much lower, only about 25 % of that (Figure 4 f1).

To obtain information on the adsorption strength of CO on the Ru/TiO_2 catalysts, we carried out isothermal desorption measurements in N_2 at 190 °C after the reaction, following changes of the CO_{ad} coverage by DRIFTS (for the resulting desorption spectra see Figure S16). The spectra recorded at the end of the isothermal desorption in N_2 desorption (dashed lines in Figure 4e) indicate that on the Ru/TiO_2-{001} the CO adlayer was almost completely removed during desorption, while on the other two catalysts absorption features are still clearly visible. A quantitative evaluation of the integrated intensity of all CO_{ad} species (see Figure 4 f2) shows that in the first 10 min the CO_{ad} coverage decreased by 72 % on Ru/TiO_2-{001}, while for Ru/TiO_2-{100} and Ru/TiO_2-{101} it decreased only by about 45 %. Furthermore, after 1000 min only 2 % of the initial CO_{ad} remained on Ru/TiO_2-{001}, while on Ru/TiO_2-{100} and Ru/TiO_2-{101} we could still detect 25 % of the initial intensity/ CO_{ad} coverage. These results point to a significantly weaker CO adsorption on the Ru NPs of the Ru/TiO_2-{001} catalyst; they also fit well to the much smaller CO_{ad} coverage observed under reaction conditions on this catalyst compared to those on the other two catalysts. The higher CO binding strength and the resulting higher CO_{ad} coverage during reaction on the Ru/TiO_2-{100} and Ru/TiO_2-{101} catalysts compared to Ru/TiO_2-{001} can be rationalized by stronger electronic metal–support interactions (EMSIs) between the partly reduced TiO_2 NCs in the Ru/TiO_2-{100} and Ru/TiO_2-{101} catalysts compared to the much less reduced TiO_2 NCs in Ru/TiO_2-{001}. This results in a stronger stabilization of the flat Ru NPs with more undercoordinated Ru sites than that obtained for the hemispherical Ru NPs on Ru/TiO_2-{001}, and likely also in a more pronounced electronic modification of the Ru surface atoms due to the stronger EMSIs.

In summary, we have successfully fabricated highly active and stable Ru/TiO_2-{100} and Ru/TiO_2-{101} catalysts for the selective CO methanation by morphology engineering of the TiO_2 support. The larger number of stable O-vacancy (surface) defects present on the Ru/TiO_2-{100} and Ru/TiO_2-{101} catalysts results in pronounced EMSIs and stabilizes highly dispersed, flat Ru NPs on these catalysts. In contrast, Ru NPs supported on TiO_2-{001} NCs with much lower surface defect densities are lacking this stabilization and undergo a gradual shape change from flat NPs, directly after reduction, to hemispherical/spherical shapes during the reaction. This and the related lower electronic modifications of the Ru surface atoms result in a continuous, slow deactivation of the Ru/TiO_2-{001} catalyst, while the other two catalysts retained their high activity. These findings underline the potential of

oxide morphology engineering in heterogeneous catalysis and open up possibilities for the development of highly stable Ru/TiO_2 catalysts, suitable for application.

Acknowledgements

S.C. is grateful for a fellowship from the Ministry of Science, Research and Arts of the State of Baden-Württemberg. W.H. acknowledges financial support of the National Natural Science Foundation of China (21525313) and the Changjiang Scholars Program of the Ministry of Education of China. We thank the ESRF for beamtime allocation (ID24 beamline) and Dr. Manuel Caballero and Dr. Sakura Pascarelli for their support. We also thank Dr. T. Diemant and S. Blessing (Ulm University) for XPS and XRD measurements.

Conflict of interest

The authors declare no conflict of interest.

Keywords: CO methanation · metal–support interactions · morphology engineering · particle shape · Ru/TiO_2

How to cite: *Angew. Chem. Int. Ed.* **2019**, *58*, 10732–10736
Angew. Chem. **2019**, *131*, 10842–10847

[1] A. Chen, T. Miyao, K. Higashiyama, H. Yamashita, M. Watanabe, *Angew. Chem. Int. Ed.* **2010**, *49*, 9895–9898; *Angew. Chem.* **2010**, *122*, 10091–10094.
[2] G. Ercolino, M. A. Ashraf, V. Specchia, S. Specchia, *Appl. Energy* **2015**, *143*, 138–153.
[3] S. Takenaka, T. Shimizu, K. Otsuka, *Int. J. Hydrogen Energy* **2004**, *29*, 1065–1073.
[4] P. Panagiotopoulou, D. I. Kondarides, X. E. Verykios, *Appl. Catal. B* **2009**, *88*, 470–478.
[5] C. Galletti, S. Specchia, G. Saracco, V. Specchia, *Chem. Eng. Sci.* **2010**, *65*, 590–596.
[6] P. Djinović, C. Galletti, S. Specchia, V. Specchia, *Top. Catal.* **2011**, *54*, 1042–1053.
[7] S. Eckle, Y. Denkwitz, R. J. Behm, *J. Catal.* **2010**, *269*, 255–268.
[8] A. M. Abdel-Mageed, S. Eckle, R. J. Behm, *J. Am. Chem. Soc.* **2015**, *137*, 8672–8675.
[9] A. M. Abdel-Mageed, D. Widmann, S. E. Olesen, I. Chorkendorff, J. Biskupek, R. J. Behm, *ACS Catal.* **2015**, *5*, 6753–6763.
[10] A. M. Abdel-Mageed, D. Widmann, S. E. Olesen, I. Chorkendorff, R. J. Behm, *ACS Catal.* **2018**, *8*, 5399–5414.
[11] S. Chen, A. M. Abdel-Mageed, C. Gauckler, S. E. Olesen, I. Chorken-dorff, R. J. Behm, *J. Catal.* **2019**, *373*, 103–115.
[12] A. M. Abdel-Mageed, S. Eckle, R. J. Behm, *J. Catal.* **2016**, *335*, 79–94.
[13] A. M. Abdel-Mageed, D. Widmann, S. Eckle, R. J. Behm, *ChemSusChem* **2015**, *8*, 3869–3881.
[14] K. Zhou, Y. Li, *Angew. Chem. Int. Ed.* **2012**, *51*, 602–613; *Angew. Chem.* **2012**, *124*, 622–635.
[15] Z.-A. Qiao, Z. Wu, S. Dai, *ChemSusChem* **2013**, *6*, 1821–1833.
[16] Z. Zhang, H. Wu, Z. Yu, R. Song, K. Qian, X. Chen, J. Tian, W. Zhang, W. Huang, *Angew. Chem. Int. Ed.* **2019**, *58*, 4276–4280; *Angew. Chem.* **2019**, *131*, 4320–4324.
[17] W. Huang, *Acc. Chem. Res.* **2016**, *49*, 520–527.
[18] S. Chen, B. Zhang, D. Su, W. Huang, *ChemCatChem* **2015**, *7*, 3290–3298.
[19] D. Li, S. Chen, R. You, Y. Liu, M. Yang, T. Cao, K. Qian, Z. Zhang, J. Tian, W. Huang, *J. Catal.* **2018**, *368*, 163–171.
[20] X. Han, Q. Kuang, M. Jin, Z. Xie, L. Zheng, *J. Am. Chem. Soc.* **2009**, *131*, 3152–3153.
[21] L. Liu, X. Gu, Z. Ji, W. Zou, C. Tang, F. Gao, L. Dong, *J. Phys. Chem. C* **2013**, *117*, 18578–18587.
[22] S. Chen, D. Li, Y. Liu, W. Huang, *J. Catal.* **2016**, *341*, 126–135.
[23] S. Chen, T. Cao, Y. Gao, D. Li, F. Xiong, W. Huang, *J. Phys. Chem. C* **2016**, *120*, 21472–21485.
[24] A. M. Karim, V. Prasad, G. Mpourmpakis, W. W. Lonergan, A. I. Frenkel, J. G. Chen, D. G. Vlachos, *J. Am. Chem. Soc.* **2009**, *131*, 12230–12239.
[25] A. Jentys, *Phys. Chem. Chem. Phys.* **1999**, *1*, 4059–4063.
[26] H. Liu, H. T. Ma, X. Z. Li, W. Z. Li, M. Wu, X. H. Bao, *Chemosphere* **2003**, *50*, 39–46.
[27] C. P. Kumar, N. O. Gopal, T. C. Wang, M. S. Wong, S. C. Ke, *J. Phys. Chem. B* **2006**, *110*, 5223–5229.
[28] K. Hadjiivanov, J.-C. Lavalley, J. Lamotte, F. Maugé, J. Saint-Just, M. Che, *J. Catal.* **1998**, *176*, 415–425.
[29] B. T. Loveless, C. Buda, M. Neurock, E. Iglesia, *J. Am. Chem. Soc.* **2013**, *135*, 6107–6121.

Manuscript received: April 4, 2019
Accepted manuscript online: May 16, 2019
Version of record online: June 27, 2019

